Chinese Chemical Letters 33 (2022) 4710–4714

Contents lists available at ScienceDirect

Chinese Chemical Letters

journal homepage: www.elsevier.com/locate/cclet

# Dissection the endocytic routes of viral capsid proteins-coated upconversion nanoparticles by single-particle tracking

Yujun Ning[a,b], Lin Wei[c], Shen Lin[b], Yifan Jiang[d,e], Naidong Wang[d,*], Lehui Xiao[b,*]

[a] College of Chemistry, Zhengzhou University, Zhengzhou 450001, China
[b] State Key Laboratory of Medicinal Chemical Biology, Tianjin Key Laboratory of Biosensing and Molecular Recognition, College of Chemistry, Nankai University, Tianjin 300071, China
[c] College of Chemistry and Chemical Engineering, Hunan Normal University, Changsha 410081, China
[d] College of Veterinary Medicine, Hunan Agricultural University, Changsha 410128, China
[e] School of Chemistry and Chemical Engineering, Henan Normal University, Xinxiang 453007, China.

ARTICLE INFO

*Article history:*
Received 24 September 2021
Revised 26 October 2021
Accepted 30 December 2021
Available online 4 January 2022

*Keywords:*
Upconversion nanoparticles
Viral capsid proteins
Single-particle tracking
Hepatoma cells
Endocytosis

ABSTRACT

Real-time exploring the cellular endocytic pathway of viral capsid proteins (VCPs) functionalized nanocargos at the single-particle level can provide deep insight into the kinetic information involved in virus infection. In this work, porcine circovirus type 2 (PCV2) VCPs with different functions are modified onto the surface of upconversion nanoparticles (VCPs-UCNPs) to investigate the cellular internalization process in real-time. Clathrin-mediated endocytosis is found to be the essential uptake mechanism for these VCPs-UCNPs. Besides, it is verified that $P_1$-UCNPs (PCV2 VCPs with nuclear localization signal, namely $P_1$) can be easily assembled close to the perinuclear area, which is different from that of $P_2$-UCNPs (PCV2 VCPs without nuclear localization signal, namely $P_2$). Interestingly, multistep entry processes are observed. Particularly, confined diffusion is observed during the transmembrane process. The intracellular transport of VCPs-UCNPs is dependent on microtubules toward the cell interior. During this process, $P_1$-UCNPs display increased velocities with active transport, while diffusion much faster around the perinuclear area. But for $P_2$-UCNPs, there are only two phases involved in their endocytosis process. This study presents distinct dynamic mechanisms for the nanocargos with different functions, which would make a useful contribution to the development of robust drug delivery systems.



Porcine circovirus type 2 (PCV2), a member of genus circovirus in the family Circoviridae, has been identified as the pathogen of porcine circovirus-associated disease, such as post-weaning multisystemic wasting syndrome, porcine dermatitis and nephropathy syndrome, respiratory distress, and acute pulmonary edema [1]. With increasing frequency of swine flu outbreaks in most swine-producing countries, PCV2 is regarded as a potential emerging pathogen that poses a global threat to livestock and human public health [2]. Therefore, it is urgently required to have a deep understanding of the virus invasion mechanism, which can subsequently afford new insight into the development of novel vaccines.

Recently, great efforts have been made to explore the mechanisms of virus invasion process [3]. These researches are mainly focusing on ensemble spectroscopic measurements or fixed cell imaging [4–6], which can only provide global information about the average states of the whole population of viruses, ignoring differences between single virus and the dynamics in the infection process. It is worth mentioning that there are multiple steps involved in the infection process. For example, virus invading into host cells is the first step of infection, which is a crucial target for therapeutic intervention. However, less is known about the detailed mechanism of the whole entry process.

Single-particle tracking (SPT) in living cells not only contributes to visualize the entry process at the single-virus level, but also facilitates to elucidate the dynamic virus-host cell interaction *in vivo* [7–9]. Nowadays, with the development of protein extraction technology, self-assembled virus-like particles (VLPs) with features of uniform size, excellent biocompatibility and easy functionalization have been widely employed as drug carriers in gene therapies and other fields [10]. However, in biological systems, VLPs are not stable due to their hollow nanostructure. Thanks to the development of nanometer-sized materials, rigid nanoparticles are available as carriers to overcome above shortcomings [11,12]. Among these nanocargos, fluorescent nanoparticles are generally

* Corresponding authors.
*E-mail addresses:* naidongwang@hunau.edu.cn (N. Wang), lehuixiao@nankai.edu.cn (L. Xiao).

https://doi.org/10.1016/j.cclet.2021.12.084
1001-8417/

used as labeling agents [13–15]. For instance, with SPT, Sun *et al.* marked influenza virus with inorganic semiconductor nanocrystal quantum dots (QDs) and successfully revealed the endocytic pathway in detail [13]. In general, the endocytosis pathway for virus uptaken can be classified into macropinocytosis, clathrin- and caveolin-mediated endocytosis, but relevant mechanisms have not been clearly elucidated [16,17]. As for PCV2, G. Misinzo *et al.* found that the movement of PCV2/VLPs was significantly inhibited in cells lacking of chondroitin sulfate B or heparan sulfate receptors [18]. However, in 3D4/31 mononuclear cell lines, PCV2 binds to clathrin protein and then invades the cell [19]. The above studies indicate that the impregnation mechanisms may vary in different cell lines. Therefore, a comprehensive diagram of PCV2 entry process remains to be depicted. In order to dissect the capability of long-time tracking PCV2 infection process, fluorescent nanoparticles with good photo-stability and stronger light emission are required when adopted as the labeling agents. Compared with QDs, upconversion fluorescent nanoparticles (UCNPs) with good photostability have drawn great attentions. Besides, UCNPs also possess large anti-Stokes shift, sharp emission bandwidth, low cytotoxicity, and high chemical stability [20–24]. Particularly, compared with the noble metal nanoparticles, the deep near-infrared (NIR) light excitation enables the effective reduction of background noise from biological samples, which makes UCNPs good candidates for single-particle imaging in complex biological environment.

Herein, we dissected the cellular translocation process of PCV2 viral capsid proteins (with or without nuclear localization ability) functionalized UCNPs ($P_1$-UCNPs and $P_2$-UCNPs, respectively) in HepG2 cells. With SPT, the invasion process was investigated by analyzing the behaviors of individual particles within living cell. According to the SPT results, three steps were observed for $P_1$-UCNPs, while only two phases were found for $P_2$-UCNPs. Noticeably, the study on the mechanism of PCV2 invading human cells contributes a deep understanding on the pathogenic mechanism of PCV2, and has a great significance in the development and application of corresponding vaccines.

The synthetic procedures of VCPs-UCNPs and other experimental sections were described in Supporting information.

Firstly, we characterized the spectroscopy and microscopy of UCNPs. Recently, a variety of strategies for lanthanide-doped UCNPs fabrication have been reported [25,26]. Among these strategies, thermolysis is widely employed to prepare high quality UCNPs with narrow size distribution, excellent optical properties, and good crystallinity [27]. UCNPs prepared by thermolysis are coated with OA which is insoluble in water. Therefore, ligand exchange is required for the phase transfer. In this work, hydrophilic PAA was employed to modify the outer surface of UCNPs. OA on the surface of UCNPs could be readily replaced by PAA with carboxyl groups under ultrasonication [28]. The size of the as-prepared UCNPs is around 50 nm with a desirable uniformity in morphology as shown in the TEM image (Fig. 1a). The particles display good water dispersibility and narrow size distribution, and have an average hydrodynamic size of ~58 nm as confirmed by DLS measurement. In addition, $Yb^{3+}$ and $Er^{3+}$ are sensitizer and activator, and account for 18% and 2% of doping ratio in the UCNPs, respectively. Therefore, UCNPs can emit ~550 nm green fluorescence under 980 nm cw laser irradiation (Fig. 1b).

Since the surface of UCNPs is modified with PAA while there are lots of positively charged arginine in PCV2, successful conjugation of PCV2 VCPs onto the UCNPs surface should increase the surface charge on UCNPs. As expected, after the conjugation process, zeta potential of $P_1$-UCNPs and $P_2$-UCNPs increased to $-23.82 \pm 1.22$ and $-25.48 \pm 3.57$ mV, respectively, which is much higher over the particles without protein modification ($-37.70 \pm 4.58$ mV) (Fig. 1c). In order to further assess the long-time tracking ability of these UCNPs, single-particle fluorescence imaging experiments were carried out at a home-built fluorescence microscope to evaluate the optical properties of these UCNPs at the single-particle level. As shown in Fig. 1d, there is no photo-bleaching or photo-blinking taking place within 30 s from those UCNPs. Inspired by the above optical merits, UCNPs designed herein should have promising potentials for long-time SPT.

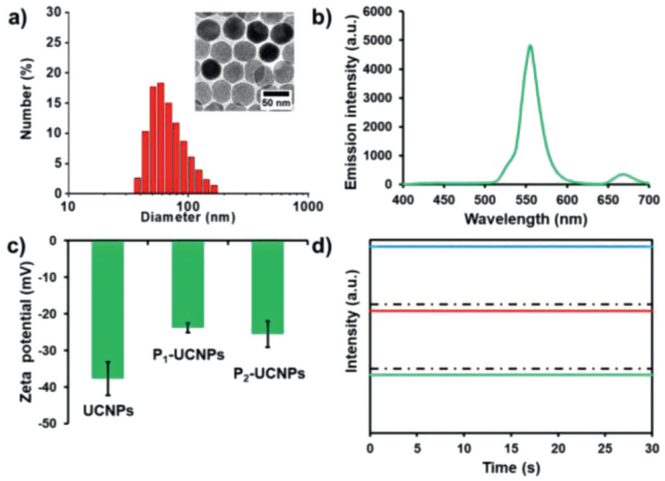


**Fig. 1.** (a) The hydrodynamic size distribution of UCNPs. Inset is the corresponding TEM image with a scale bar of 50 nm. (b) The fluorescence emission spectrum of UCNPs. (c) Zeta potentials of UCNPs, $P_1$-UCNPs and $P_2$-UCNPs. (d) Representative fluorescence intensity tracks of individual UCNPs as a function of time.

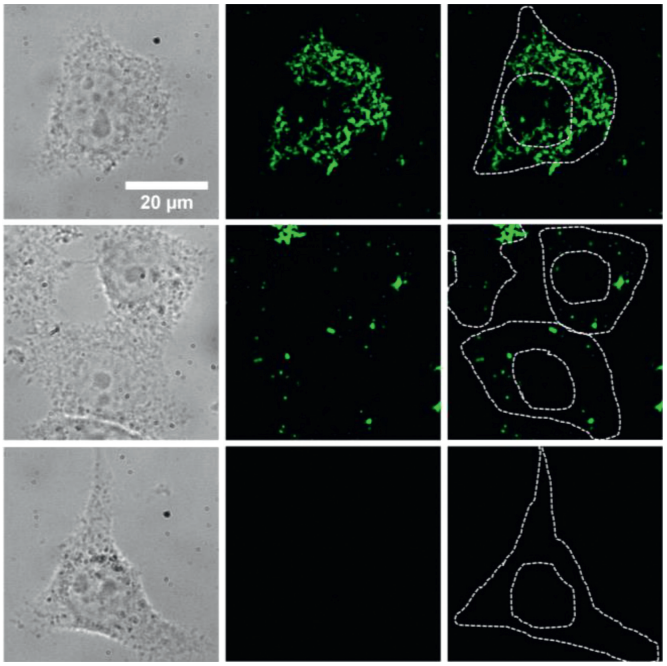


**Fig. 2.** The fluorescence microscopic characterization of HepG2 cells co-cultured with $P_1$-UCNPs (top row), $P_2$-UCNPs (middle row), and UCNPs (bottom row) at 37 °C for 6 h. The images from left to right are the bright-field, fluorescence and fluorescence images with cell outline, respectively. Scale bar: 20 μm.

Secondly, we investigated the dynamic distributions of VCPs-UCNPs in living cells. The functions of these two VCPs-UCNPs were further evaluated through quantitatively analyzing the dynamic distributions of these particles in living cells. VCPs-UCNPs were co-cultured with HepG2 cells for 6 h and then imaged with fluorescence microscope under the excitation at 980 nm. As shown in Fig. 2, obvious fluorescent signals are found from the cells co-cultured with $P_1$-UCNPs. Fluorescent signals from $P_1$-UCNPs with

nuclear localization tags were not only present in the cytoplasm, but also partially present near or around the nucleus. However, signals from $P_2$-UCNPs without nuclear localization tags only existed in the cytoplasm. In contrast to above two samples, very few UCNPs without the conjugation of VCPs existed in the cells and could be almost ignored. These results suggested that, with the same co-culture time, VCPs can facilitate particles entering cells. Besides, $P_1$-UCNPs with nuclear localization tags can target the nucleus and lead to a remarkably faster internalization rate than that of $P_2$-UCNPs.

Afterward, we investigated the uptake efficiency of VCPs-UCNPs by HepG2 cells at different time points. HepG2 cells were co-cultured with the same concentration of $P_1$-UCNPs, $P_2$-UCNPs and UCNPs at 37 °C for 2, 4 and 6 h, respectively, Figs. S1a–c (Supporting information). By using the mean fluorescence intensity of single UCNP as the reference, the number of UCNPs uptake by the cell under different co-culture time could be calculated roughly. The statistical results are shown in Fig. S1d (Supporting information). As time went on, the number of fluorescent particles within the cell increased significantly. Initially, the particles located at the cell surface. Over time, $P_1$-UCNPs and $P_2$-UCNPs started to appear in the cytoplasm, while the fluorescent signals of UCNPs were mostly locating at the boundary of cell membrane. In addition, by comparing the uptake process from these samples, one thing that deserved our attention was that the cellular uptake rate of $P_1$-UCNPs was significantly faster than that of $P_2$-UCNPs, while the rate of UCNPs is the lowest, which indicates that VCPs facilitate particles internalization.

Then, we explored the clathrin-dependent endocytosis of VCPs-UCNPs. Early studies have shown that viruses can enter cells by endocytosis, which may occur *via* several mechanisms, such as clathrin-mediated, caveolae-mediated, clathrin- and caveolae-independent endocytosis, and macropinocytosis [29]. To disclose the cellular uptake mechanism, we monitored the cellular uptake process of VCPs-UCNPs through the addition of endocytosis inhibitors. At 37 °C, cells were co-cultured directly with $P_1$- and $P_2$-UCNPs, respectively. After 6 h, their fluorescence and bright-field images were recorded and shown in Fig. S2a (Supporting information). For comparison, HepG2 cells were treated with dynasore (an inhibitor of dynamin for clathrin-mediated endocytosis) and genistein (an inhibitor of tyrosine protein kinase for caveolae-mediated endocytosis) for 1 h, respectively, and then were co-cultured with the samples under the same conditions for 6 h. The optical images are shown in Figs. S2b and c (Supporting information), respectively. By comparing the fluorescent images with and without inhibitors, it was found that the cells treated with dynasore had significantly reduced uptake efficiency while the uptake efficiency of the cells treated with genistein did not change significantly. In order to further explain the results quantitatively, the fluorescence intensity changes with and without the inhibitor treatment were statistically analyzed in the same way as described above, and the results were shown in Fig. S2d (Supporting information). According to the statistical results, the cells treated with dynasore had significantly lower uptake efficiency than those treated with genistein or without the inhibitor. Consistent with the aforementioned results, the main way of VCPs-UCNPs entering cells was clathrin-mediated endocytosis, whilst, weak green fluorescent signal could be detected in HepG2 cells when treated with dynasore, suggesting that other mechanisms should be involved in this process.

Finally, we tracked VCPs-UCNPs entry into cells with SPT in real time. To dissect the cellular uptake process in detail, SPT was performed to visualize the internalization process from single VCPs-UCNP, starting with their attachment to the cell membrane, followed by the uptake process, as well as intracellular trafficking, *etc.* In the acquired image sequences, the fluorescent particles can be identified as green spots on a dark background. Each frame in the video is a representative position of the particles at a certain time point. By extracting the corresponding x and y coordinates from all frames, the trajectories of particles were revealed.

Fig. 3a shows the real-time fluorescence images of $P_1$-UCNPs entering into the cell. The particles quickly assembled and attached to the cell membrane during the initial invasion process, penetrated across the membrane and finally targeted the vicinity of the nucleus. To dissect the infection pathway unambiguously, the trajectories of different phases are marked with different colors in Fig. 3b. In these figures, three phases can be clearly distinguished. Qualitatively, $P_1$-UCNPs first adsorbed on the membrane, then targeted the vicinity of the nucleus by directional movement, and finally moved near the nucleus. In order to quantitatively explain the motion of $P_1$-UCNPs, mean squared displacement (MSD) was calculated and fitted with the equation of $\mathrm{MSD} = 4Dt^{\alpha}$ ,where $D$ is the diffusion coefficient, $\alpha$ is diffusion exponent and $t$ is the lag time, respectively (Fig. 3c). Consistent with the result of the trajectory diagram, the exponent $\alpha$ calculated from the three stages of $P_1$-UCNPs dynamic invasion is 0.90, 1.02 and 1.22, respectively. The results meant that the initial binding movement of particles on the cytomembrane was subdiffusion, demonstrating that the nanocargos were confined on the cell membrane initially. Besides, the movement of the next two stages behaved similarly to superdiffusion, especially the last process [30]. Subsequently, we investigated the mechanisms associated with the transport quantitatively. It was found that the rate of directional movement and diffusion around the nucleus of $P_1$-UCNPs was significantly accelerated, which can be quantitatively illustrated by combining the instantaneous velocities in Fig. 3d with their statistics in Figs. 3e–g. It was found that the average velocities of the three invasion stages were $0.04 \pm 0.02$, $0.05 \pm 0.04$, and $0.24 \pm 0.18$ μm/s, respectively. The movement in phase I was slowest and characterized by a narrower velocity distribution, which could be speculated that the particles were blocked by the cell membrane and interacting with the cytomembrane. Besides, the results in Fig. S2 (Supporting information) suggested that the movement was mainly clathrin-mediated. As for phase II, the velocity distribution was broader than that of phase I. Combined with the fact that $\alpha$ calculated from the phase II was 1.02, it can be deduced that the particles displayed active and directional transport along microtubules. In the phase III, the particles showed the highest instantaneous velocity with a quite broad distribution. From these data, we concluded that the velocity of $P_1$-UCNPs migration gradually increased during the process of cell invasion, demonstrating that $P_1$-UCNPs entered HepG2 cells by means of active transport, and eventually accumulated in the perinuclear area with a fast and random diffusion.

The typical trajectory of $P_2$-UCNPs is shown in Fig. 4a. From the trajectory, we found that there were only two stages of dynamic invasion process for $P_2$-UCNPs, namely adsorption on the cytomembrane and directional migration within the cell, while the third stage was not observed as $P_1$-UCNPs did. The MSD calculated from the trajectory is shown in Fig. 4b. As we can see, the MSD exhibits a linear relationship with lag time in the double logarithmic plot, and the exponent values of these two stages are 0.94 and 1.10, respectively. It was demonstrated that the migration rule of $P_2$-UCNPs in the cell was similar to that of $P_1$-UCNPs, whereas there was no nuclear localization signal in comparison with $P_1$ protein. The instantaneous rate and velocity statistics of $P_2$-UCNPs were further calculated (Figs. 4c–e). As shown in Figs. 4d and e, the instantaneous rate increased after entering the cytoplasm. Combined with Fig. S2d, it was proved that the mechanism of $P_2$-UCNPs entering HepG2 cells by active transport was mainly clathrin-mediated. Based on the findings in this study, VCPs-UCNPs enter HepG2 cells through clathrin-mediated endocytosis. Follow-

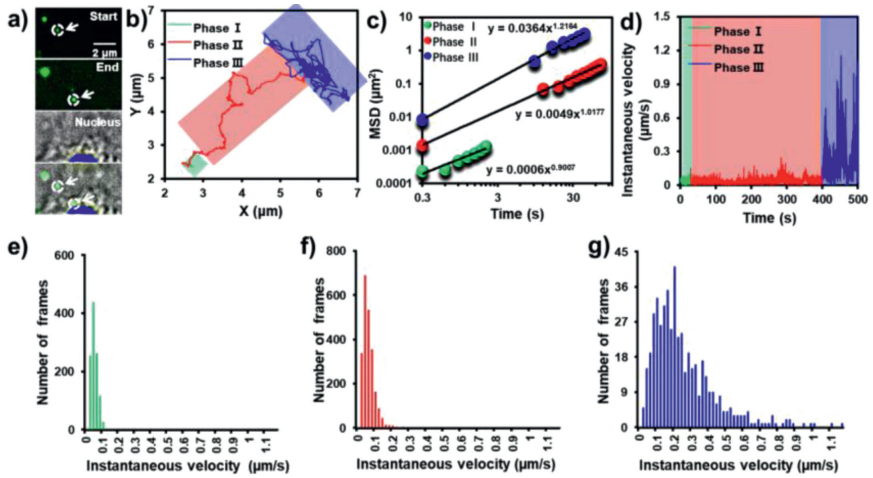


**Fig. 3.** (a) Real-time imaging of the entry of $P_1$-UCNPs into HepG2 cell, (b) trajectories, and (c) instantaneous velocity of $P_1$-UCNPs. (d) The double logarithmic plot of MSD from $P_1$-UCNPs as a function of lag time. (e–g) Histograms of the instantaneous velocity distributions during phase I, II and III, respectively.

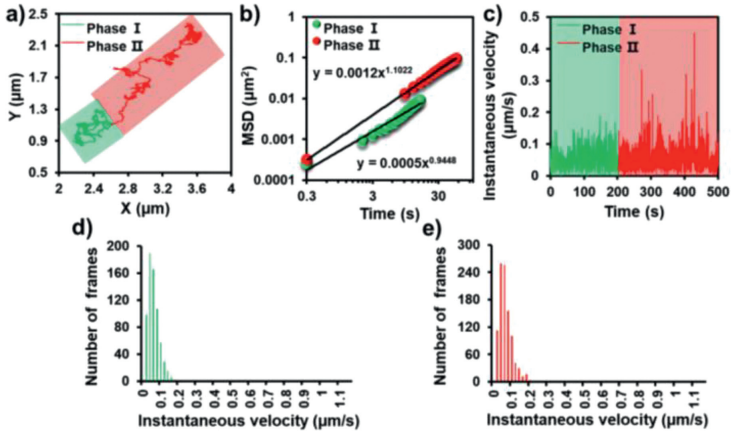


**Fig. 4.** (a) Trajectories, (b) instantaneous velocity and (c) the double logarithmic plot of MSD from $P_2$-UCNPs as a function of lag time. (d, e) Histograms of the instantaneous velocity distributions during phase I and II, respectively.

ing endocytosis, the particles move into the cytoplasm and then behave directionally along microtubes. In addition, $P_1$-UCNPs can target the nucleus, but $P_2$-UCNPs can not, as illustrated in Fig. S3 (Supporting information). Therefore, our study may aid in the investigation of virus invasion mechanisms and the development of inhibitors to block the PCV2 invading HepG2 cells.

In summary, in this work, by taking the advantage of the unique optical properties of UCNPs, the cellular migration behavior of VCPs-UCNPs was systematically studied. The distribution and location of VCPs-UCNPs in HepG2 cells were revealed by single-particle fluorescence imaging. The intracellular translocation process is strongly affected by the functionality of VCPs. With the modification of nuclear localization signal in VCPs, $P_1$-UCNPs accumulated near the nucleus after 2 h of incubation. However, $P_2$-UCNPs did not show noticeable nuclear targeting capability even with similar directional movement within the cell as that of $P_1$-UCNPs. These results would provide new insight into the intracellular dynamics of PCV2 VCPs and also afford deep understanding on virus pathogenesis.

## Declaration of competing interest

The authors declare that they have no known competing financial interests or personal relationships that could have appeared to influence the work reported in this paper.

## Acknowledgements

The authors are thankful for financial support from the National Natural Science Foundation of China (Nos. 22174079, 21974073).

## Supplementary materials

Supplementary material associated with this article can be found, in the online version, at doi:10.1016/j.cclet.2021.12.084.

## References

[1] J. Segalés, Virus Res. 164 (2012) 10–19.
[2] P. Alarcon, J. Rushton, B. Wieland, Prev. Vet. Med. 110 (2013) 88–102.
[3] S. Millecamps, J.P. Julien, Nat. Rev. Neurosci. 14 (2013) 161–176.
[4] S.B. Sieczkarski, G.R. Whittaker, J. Virol. 76 (2002) 10455–10464.
[5] E.D. Vries, R.P.D. Vries, M.J. Wienholts, et al., Proc. Natl. Acad. Sci. U. S. A. 109 (2012) 7457–7462.
[6] R.S.B. Milne, A.V. Nicola, J.C. Whitbeck, et al., J. Virol. 79 (2005) 6655–6663.
[7] K. Miyauchi, Y. Kim, O. Latinovic, et al., Cell 137 (2009) 433–444.
[8] S.L. Liu, Z.L. Zhang, Z.Q. Tian, et al., ACS Nano 6 (2012) 141–150.
[9] Y. Ma, X. Wang, H. Liu, et al., Anal. Bioanal. Chem. 411 (2019) 4445–4463.
[10] Y. Ma, R.J.M. Nolte, J.J.L.M. Cornelissen, Adv. Drug Deliv. Rev. 64 (2012) 811–825.
[11] N.L. Goicochea, M. De, V.M. Rotello, et al., Nano Lett. 7 (2007) 2281–2290.
[12] S.Y. Lee, J.S. Lim, M.T. Harris, Biotechnol. Bioeng. 109 (2012) 16–30.
[13] E.Z. Sun, A.A. Liu, Z.L. Zhang, et al., ACS Nano 11 (2017) 4395–4406.
[14] L.L. Huang, P. Zhou, H.Z. Wang, et al., Chem. Commun. 48 (2012) 2424–2426.
[15] L.L. Huang, K. Liu, Q. Zhang, et al., Anal. Chem. 89 (2017) 11620–11627.
[16] D. Blaas, Wien. Med. Wochenschr. 166 (2016) 211–226.

[17] A.V. Nicola, H.C. Aguilar, J. Mercer, et al., Adv. Virol. 2013 (2013) 469538.
[18] G. Misinzo, P.L. Delputte, P. Meerts, et al., J. Virol. 80 (2006) 3487–3494.
[19] G. Misinzo, P. Meerts, M. Bublot, et al., J. Gen. Virol. 86 (2005) 2057–2068.
[20] D. Zhang, L. Wei, M. Zhong, et al., Chem. Sci. 9 (2018) 5260–5269.
[21] X. Li, L. Wei, L. Pan, et al., Anal. Chem. 90 (2018) 4807–4814.
[22] Y. Dai, H. Xiao, J. Liu, et al., J. Am. Chem. Soc. 135 (2013) 18920–18929.
[23] Q. Xing, N. Li, Y. Jiao, et al., RSC Adv. 5 (2015) 5269–5276.
[24] L. Wang, H. Dong, Y. Li, et al., J. Am. Chem. Soc. 136 (2014) 4480–4483.
[25] H.T. Wong, M.K. Tsang, C.F. Chan, et al., Nanoscale 5 (2013) 3465–3473.
[26] M.V. DaCosta, S. Doughan, Y. Han, et al., Anal. Chim. Acta 832 (2014) 1–33.
[27] G. Chen, H. Qiu, P.N. Prasad, et al., Chem. Rev. 114 (2014) 5161–5214.
[28] F. Wang, Y. Han, S. Wang, et al., Anal. Chem. 91 (2019) 11856–11863.
[29] H. Shen, L.J. Tauzin, R. Baiyasi, et al., Chem. Rev. 117 (2017) 7331–7376.
[30] Z. Xu, L. Gao, P. Chen, et al., Soft Matter 16 (2020) 3869–3881.